Interparticle interactions in magnetic core/shell nanoarchitectures

Georgia C. Papaefthymiou*
Institute of Materials Science, NCSR "Demokritos," 15310 Athens, Greece
and Department of Physics, Villanova University, Villanova, Pennsylvania 19085, USA

Eamonn Devlin and Athanassios Simopoulos†
Institute of Materials Science, NCSR "Demokritos," 15310 Athens, Greece

Dong Kee Yi,‡ Siti Nurhanna Riduan, Su Seong Lee, and Jackie Y. Ying
Institute of Bioengineering and Nanotechnology, 31 Biopolis Way, The Nanos, Singapore 138669, Singapore
(Received 24 June 2008; revised manuscript received 27 January 2009; published 6 July 2009)

Magnetic and Mössbauer measurements are reported on single-crystalline monodispersed γ-Fe_2O_3 nanoparticles of 12.5 nm diameter, coated with multiple silica and mesoporous silica layers of various thicknesses. The high crystallinity and monodispersity of the samples allow resolution of the tetrahedral (A) and octahedral [B] iron sites of the spinel structure of maghemite. The precisely tuned silica coating thickness offers controlled, homogeneous magnetic dilution with the sample magnetic volume fraction ranging from 1 to 0.002, leading to various degrees of interparticle dipole-dipole interaction strength. Analysis of the zero-field-cooled magnetization data shows that dipole-dipole interactions increase the superparamagnetic energy barrier. The relevant magnetic parameters, for both the individual particles (K_{eff}) and the particle assemblies (U_{int}), are determined within the framework of weak and strong dipolar-interaction models. At low temperatures, the steepness of the magnetic hyperfine field reduction with increasing temperature in the strongly interacting particle assemblies is examined within the context of the collective magnetic-excitations model.

DOI: 10.1103/PhysRevB.80.024406 PACS number(s): 75.50.Tt, 75.75.+a, 76.80.+y

I. INTRODUCTION

The magnetic properties of nanoparticles are of interest in fundamental studies of their physics and in a broad spectrum of technological applications.[1–8] Many theoretical and experimental studies have addressed properties specific to nanoparticles such as surface spin canting, the macroscopic quantum tunneling of magnetization, spin reversal, and magnetic-relaxation mechanisms.[9–21]

Elucidation of such intrinsic magnetic properties and the validation of the proposed theoretical models depend critically on the quality of experimental samples and their amenability to detailed micromagnetic characterization. Many of the early experimental studies were performed on samples with broad particle-size distributions and individual particles of poor crystallinity. In recent years, significant effort has been devoted toward the development of advanced synthesis techniques to produce monodispersed highly crystalline magnetic nanoparticles.[22]

The study of the magnetic properties of an ensemble of nanoparticles requires the determination of not only the intrinsic magnetic properties of the individual particles but also the type and strength of interparticle interactions. If the particles are in close proximity, they will interact magnetically via two distinct mechanisms: magnetic exchange across particle boundaries in contact and dipole-dipole interactions.[23–27] The latter, being long-range interactions, are present in most particle assemblies. High magnetic dilution is required for dipole-dipole interactions to become negligible. Many experimental studies on interparticle interactions have employed frozen ferrofluids,[28] granular samples of immiscible metals of varying magnetic volume fractions,[29] or samples prepared by cosputtering of two immiscible metals followed by thermal/annealing treatments.[30,31] In such samples, it is often difficult to control clustering over a broad range of magnetic dilution, and in the case of cosputtered metal samples, the presence of Ruderman-Kittel-Kasuya-Yosida interactions further complicates the interpretation of experimental results in relation to dipole-dipole interactions.

In this paper, we report on the interparticle magnetic interactions garnered from nanoarchitectured samples of single-crystalline γ-Fe_2O_3 nanoparticles passivated with oleic acid and subsequently coated with solid silica (SiO_2) and additionally covered with various thicknesses of mesoporous silica (MS). Transmission electron microscopy images of our samples reveal high particle crystallinity, monodispersity, and precisely controlled SiO_2 and MS coating thicknesses; these samples are of high homogeneity and are free of clustering. Since silica is nonmagnetic, controlled magnetic dilution, covering all interaction regimes from strongly interacting to noninteracting isolated γ-Fe_2O_3 magnetic nanoparticles is achieved by a systematic increase in the silica coating thickness.

The presence of iron in our samples allows sample characterization via Mössbauer spectroscopy, in addition to magnetization measurements. The combination of the two techniques probes the macromagnetic and micromagnetic properties of the samples and their dynamic spin-relaxation processes. This approach also allows for the determination of magnetic parameters, i.e., the estimation of the strength of the dipolar interactions in the particle assembly and the magnetic anisotropy constant of individual particles, in the regimes of strongly and weakly interacting particles, respectively.

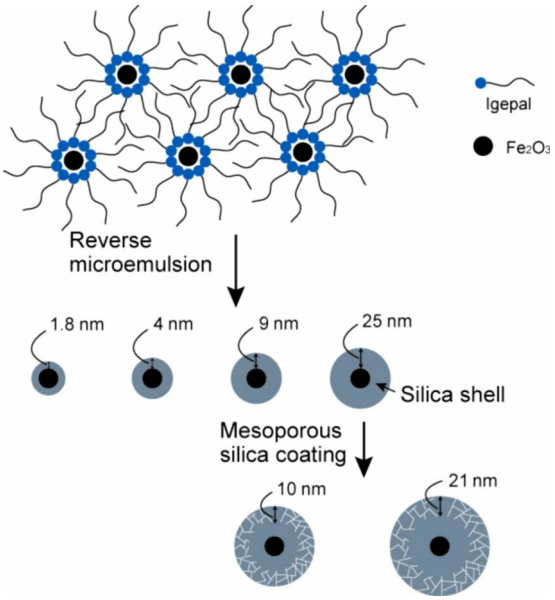

FIG. 1. (Color online) Schematic of the synthesis of γ-Fe_2O_3 nanoparticles derived by reverse microemulsion with various solid SiO_2 coating thicknesses (top, center). Further development of silica-coated γ-Fe_2O_3 nanoparticles with mesoporous silica shell (bottom).

II. MATERIALS AND METHODS

Details on the synthesis and physical characterization of the samples examined in this study have been reported elsewhere.[32] In brief, Fig. 1 depicts the synthetic route for the fabrication of the various core/shell nanoarchitectures. First, monodispersed γ-Fe_2O_3 nanoparticles with a uniform particle diameter were synthesized according to the method of Hyeon *et al.*[33] Figure 2 shows x-ray diffraction (XRD)

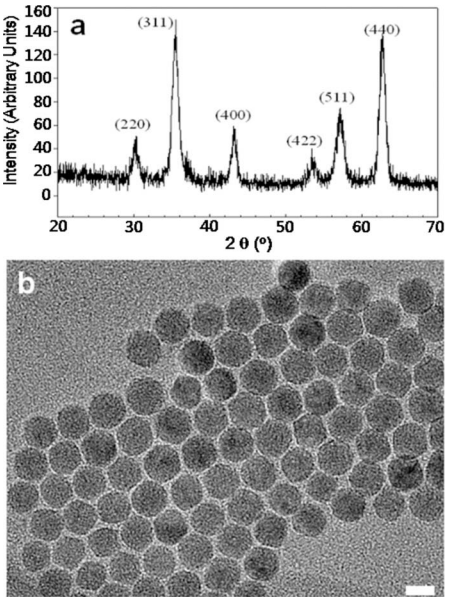

FIG. 2. (a) XRD of oleic acid-stabilized γ-Fe_2O_3 magnetic nanoparticles. (b) TEM micrographs indicating a uniform particle diameter of 12.5 nm. Scale bar=10 nm.

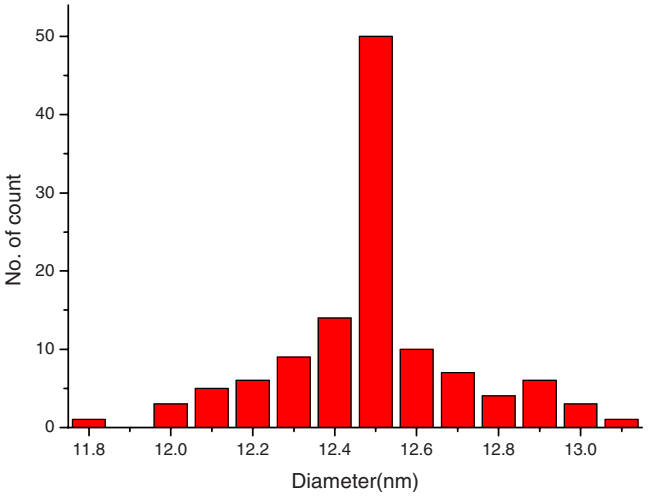

FIG. 3. (Color online) Particle-size distribution analysis of TEM micrographs of Fig. 2. Estimated particle diameter $d=(12.500\pm0.222)$ nm on 119 particles measured.

patterns and transmission electron microscopy (TEM) images of 12.5-nm-diam γ-Fe_2O_3 nanoparticles. Monodispersed single-crystalline γ-Fe_2O_3 nanoparticles were successfully obtained as illustrated in the self-assembled formation of the hexagonal superlattice in Fig. 2(b) and by the TEM particle-size distribution in Fig. 3, which established a magnetic core average diameter of (12.500 ± 0.222) nm. These particles were passivated with a thin layer of oleic acid and used as substrates to obtain silica- and MS-coated γ-Fe_2O_3 nanoparticles through water-in-cyclohexane reverse microemulsion (see Fig. 1). Representative TEM micrographs of silica/MS-coated structures are shown in Figs. 4 and 5.

In this study, the 12.5 nm γ-Fe_2O_3 nanoparticles were coated with varying thicknesses of SiO_2 and additional mesoporous silica and then used for magnetization and Mössbauer measurements in a packed powder form. A conventional transmission Mössbauer spectrometer was employed with sample temperatures varied from 4.2 K to room temperature (RT) in an Oxford Variox cryostat. The source was ^{57}Co(Rh) moving with constant acceleration at RT. Isomer shifts were given with respect to metallic iron at RT. Magnetization measurements were performed in Quantum Design physical properties measurement system (PPMS) and superconducting quantum interference device magnetometers over the same temperature range.

Architectural characteristics of the various nanoparticle samples studied in this work, labeled A–E, together with parameters derived from the magnetization measurements are given in Table I. Due to the low iron content of the samples with thicker SiO_2/MS coatings, only samples A–C were employed in Mössbauer measurements.

III. RESULTS AND DISCUSSION

The Mössbauer spectra of the 12.5 nm γ-Fe_2O_3 bare (i.e., no silica coating) nanoparticles at 4.2 K are shown in Fig. 6. The sharp absorption spectral lines observed were another

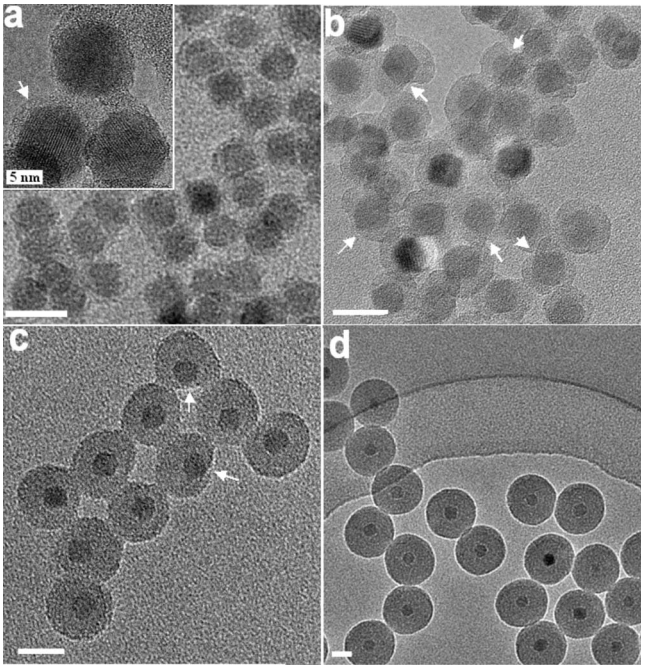

FIG. 4. TEM micrographs of 12.5 nm γ-Fe_2O_3 nanoparticles with a solid SiO_2 shell of (a) ~1.8 nm (denoted by an arrow in the high-resolution image in the inset), (b) ~4 nm, (c) ~9 nm, and (d) ~25 nm. Scale bar=20 nm, unless otherwise noted. In most cases, the SiO_2-coated γ-Fe_2O_3 nanocomposite particles are spherical and uniform in size.

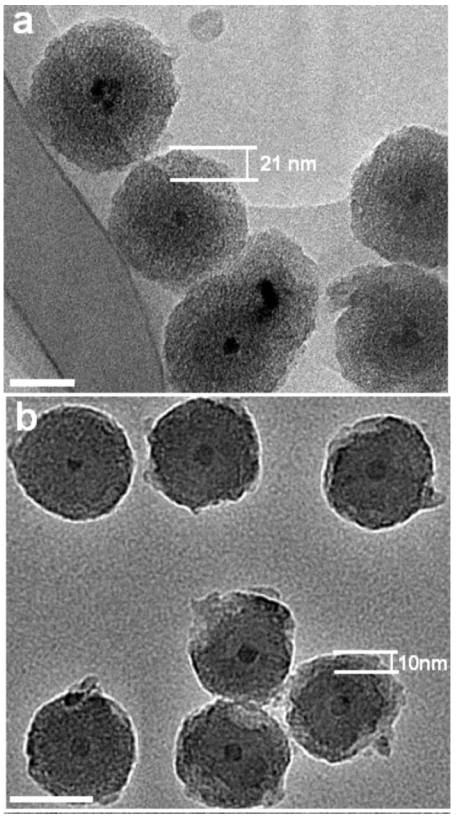

FIG. 5. TEM micrographs of 12.5 nm γ-Fe_2O_3 nanoparticles coated with 25-nm-thick solid SiO_2 shell and (a) 21-nm-thick and (b) 10-nm-thick mesoporous silica shell. Scale bar=50 nm.

manifestation of the high crystallinity of the magnetic core structure and the particle-size monodispersity of the samples illustrated above (Figs. 2 and 3). An asymmetry in both height and linewidth was observed in lines 1 and 6 of these spectra. This asymmetry arose from the resolution of the two sublattices of the spinel structure of maghemite.[34] Thus, the spectra were fitted assuming the superposition of two magnetic subsites associated with the tetrahedral (A) and octahedral [B] iron coordination sites of the spinel structure. Least squares fits gave the hyperfine parameters listed in Table II. These parameters were in agreement with the values of bulk γ-Fe_2O_3.[12]

Figure 7 shows the Mössbauer spectral temperature profile of the bare particles from 4.2 K to room temperature. As the temperature is raised above 78 K, the general form of the spectra changes from the asymmetric sextet associated with the resolution of the (A) and [B] sites to a broadened symmetric sextet. Fitting of the sextet at 150 K requires two broadened subspectra, while for 200 K and above, an additional component of intermediate magnetic relaxation must be introduced in order to account for the overall broadening of the spectra. This component increases in intensity with temperature. The spectra, however, remain magnetically split even at room temperature, albeit broadened. This arises from relaxation effects that are common in an assembly of magnetic nanoparticles. The magnetic moment of a nanoparticle fluctuates along the easy magnetization axis with a time constant $\tau = \tau_0 \exp(K_{\text{eff}} V_m / k_B T)$, where K_{eff} is the magnetic anisotropy constant, V_m is the volume of the magnetic particle, k_B is the Boltzmann constant, and T is the temperature. For a single particle of volume V_m with a spin-fluctuation time much longer than the characteristic Mössbauer time (10^{-8} s), a full magnetic hyperfine split spectrum appears (slow relaxation). As the temperature increases, this time shortens and the particle behaves as a superparamagnet displaying a singlet or a doublet spectrum (fast relaxation). At intermediate temperatures, as the fluctuating time is close to the Mössbauer time, broadened hyperfine spectra appear with typical relaxation features. For an assembly of particles with a broad particle-size distribution, both magnetic sextets and paramagnetic doublets are displayed simultaneously due to the distribution of the fluctuation times, the latter increasing at the expense of the former as the temperature increases. For a monodispersed system, as in the present case, only magnetic hyperfine spectra appear until they collapse to a doublet at a high enough temperature. The appearance of an intermediately relaxing component at temperatures above 200 K (Fig. 7) indicates that part of the system fluctuates faster than the rest. This could arise from the outer part of the particles where the inherent disorder allows for easier fluctuations. Further evidence in support of this assumption is presented below.

Figure 8 shows the Mössbauer spectra of the same particles coated with a 25-nm-thick solid silica shell. The magnetic isolation of the cores provided by the intervening silica shell resulted in faster magnetic relaxation at room temperature, leading to the observation of a collapsed, complex Mössbauer spectrum, not yet fully superparamagnetic (SP).

TABLE I. Selected magnetic parameters from magnetization measurements of 12.5 nm γ-Fe_2O_3 nanoparticles with and without silica shell. r=lower bound of nearest-neighbor interparticle distance, V_m/V =magnetic volume fraction, T_{max} at H_{app}=50 Oe, T_{Br}=bifurcation, or branching temperature.

Sample	SiO_2 and MS shell thicknesses (nm)	r (nm)	V_m/V	T_{max} (K)	T_{Br} (K)	Classification
A	0	12.5	1.0	>300	250	Strongly interacting
B	4(SiO_2)	20.5	0.227	175	185	Strongly interacting
C	25(SiO_2)	62.5	0.008	120	160	Intermediately interacting
D	25(SiO_2)+10(MS)	82.5	0.003	77	110	Weakly interacting
E	25(SiO_2)+21(MS)	104.5	0.002	75	100	Isolated

Figures 9(a)–9(c) compare the room-temperature Mössbauer spectra of the 12.5 nm magnetic nanoparticles without a SiO_2 shell, with a 4-nm-thick SiO_2 shell, and with a 25-nm-thick SiO_2 shell. The variation in the strength of the interparticle interactions was manifested in these spectra by the progressive change from slow to intermediate and fast relaxation rates with increasing silica-shell thickness, as the distance between adjacent particles (center-to-center) increased from 12.5 to 20.5 and to 62.5 nm. These distances were lower bound estimates in the packed powder samples. No superposition of magnetic six-line (slow relaxing) and quadrupolar-doublet (fast relaxing) spectra was observed in this study below room temperature. This was another clear testimony to the monodispersity of the samples, in agreement with the histogram of Fig. 3. Furthermore, the increase in the magnetic-moment fluctuation rate, with the increase in the distance between the magnetic cores, was a manifestation of the decrease in the energy barrier as the strength of the dipolar interaction decreased.

The onset of collective magnetic-relaxation phenomena was observed with increasing temperature for all three samples studied with Mössbauer spectroscopy. For the bare particles, Fig. 7 illustrates the broadening of the (A) and [B] subsite absorption lines, and the reduction in the magnitude of the internal hyperfine fields at these iron sites. The rate of magnetic hyperfine field reduction with increasing temperature for samples A, B and C is shown in Fig. 10. As expected, the reduction in field with temperature was steeper for the coated particles compared to the bare particles, due to the reduction in interparticle magnetic interaction strength. For isolated and randomly oriented superparamagnetic particles of uniaxial magnetic anisotropy such a reduction in hyperfine magnetic field value has been satisfactorily explained by the collective magnetic excitations (CMEs) model of Mørup and Topsøe.[35] The model predicts a linear reduction in field values of up to 15% from the value of the saturation field, before superparamagnetic relaxation sets in, in accordance with

$$H_{hf}(T) = H_{hf}^0(1 - k_B T/2K_{eff}V_m), \quad (1)$$

where H_{hf}^0 is the saturation hyperfine field as $T \rightarrow 0$, k_B is Boltzmann's constant, K_{eff} is the effective magnetic anisotropy energy density of the particle, V_m is the volume of the magnetic core, and T is the temperature. The slope, $\Delta H_{hf}/\Delta T = -H_{hf}^0 k_B/(2K_{eff}V_m)$, depends only on the saturation hyperfine field and the magnetic anisotropy energy of the particle and is, therefore, temperature independent. However, the presence of interparticle dipole-dipole interactions in these samples, which can be temperature dependent, renders the modeling of the reduction of the internal hyperfine magnetic field at the iron nucleus far more complex. We will return to this point later.

TABLE II. Selected Mössbauer parameters at 4.2 K for 12.5 nm γ-Fe_2O_3 nanoparticles with and without silica shell. δ=isomer shift with respect to metallic iron at RT, Γ=linewidth (half-width at half maximum), H_{hf}=hyperfine field, $\Delta H_{hf}/\Delta T$=initial slope evaluated from experimental data obtained at 4.2 and 78 K, and H_{hf}^0=saturation hyperfine field.

Sample	SiO_2 shell thickness (nm)	Site	δ (mm/s)	Γ (mm/s)	H_{hf} (kOe)	$\Delta H_{hf}/\Delta T$ (kOe/K)
		(A)	0.31(1)	0.22(1)	515(1)	−0.230
A	0	[B]	0.52(1)	0.22(1)	524(1)	−0.095
		(A)	0.34(2)	0.22(3)	512(2)	−0.240
B	4	[B]	0.51(2)	0.21(1)	524(1)	−0.095
		(A)	0.36(2)	0.22(3)	512(2)	−0.312
C	25	[B]	0.52(2)	0.22(2)	524(1)	−0.150
	CME Model	(A)			516 (H_{hf}^0)	−0.147
		[B]			525 (H_{hf}^0)	−0.150

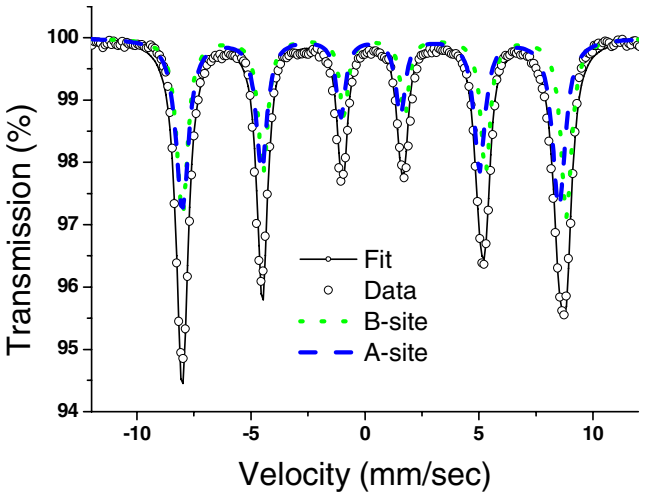

FIG. 6. (Color online) Mössbauer spectra of 12.5 nm γ-Fe_2O_3 nanoparticles (depicted in Fig. 2) at 4.2 K. The tetrahedral (---, blue) (A) sites and octahedral (···, green) [B] sites of the spinel structure are clearly resolved through spectral fitting.

To further investigate the dynamic spin-relaxation phenomena observed, complementary magnetization studies were performed on the 12.5 nm γ-Fe_2O_3 nanoparticles with and without silica coatings of various thicknesses corresponding to sample magnetic volume fractions varying in the range of 1.0–0.002. Some magnetization data (on saturation magnetization and coercivity) on these samples have already been published.[32] A saturation magnetization of ~57 emu/g was determined for the bare particles from these data. Herein we present only the zero-field-cooled (ZFC) and field-cooled (FC) magnetization curves (Fig. 11). The sample characteristics and magnetic parameters derived are summarized in Table I.

For isolated superparamagnetic particles, the maximum in the ZFC magnetization data, $T_{\max}$, gives a measure of the SP blocking temperature, T_B, at which the thermal energy equals the magnetic anisotropy energy ($K_{\text{eff}}V_m$) of the particles. For uniaxial magnetic anisotropy, the SP relaxation time is given by[13–15]

$$\tau = \tau_0 e^{(K_{\text{eff}}V_m/k_BT)}, \tag{2}$$

where τ_0 is a constant of the order of 10^{-9}–10^{-12} s, which is characteristic of the material.[36] It follows that for isolated SP particles,

$$T_{\max} = T_B = (K_{\text{eff}}V_m/k_B)/\ln(\tau_m/\tau_0), \tag{3}$$

where τ_m is the characteristic magnetization measurement time, typically 10–100 s. Thus, determination of T_B allows for estimation of the magnetic anisotropy energy density (K_{eff}) for particles of known volume (V_m).

Due to the large magnetic moments of small single-magnetic domain particles, which are 10^3–10^4 larger as compared to paramagnetic centers, dipole-dipole magnetic interaction energies between particles shift from the millikelvin regime for paramagnets to the Kelvin regime for superparamagnets. The orientational magnetic interaction energy between the magnetic moments, $\vec{\mu}_i$ and $\vec{\mu}_j$, of two magnetic particles is given by[37]

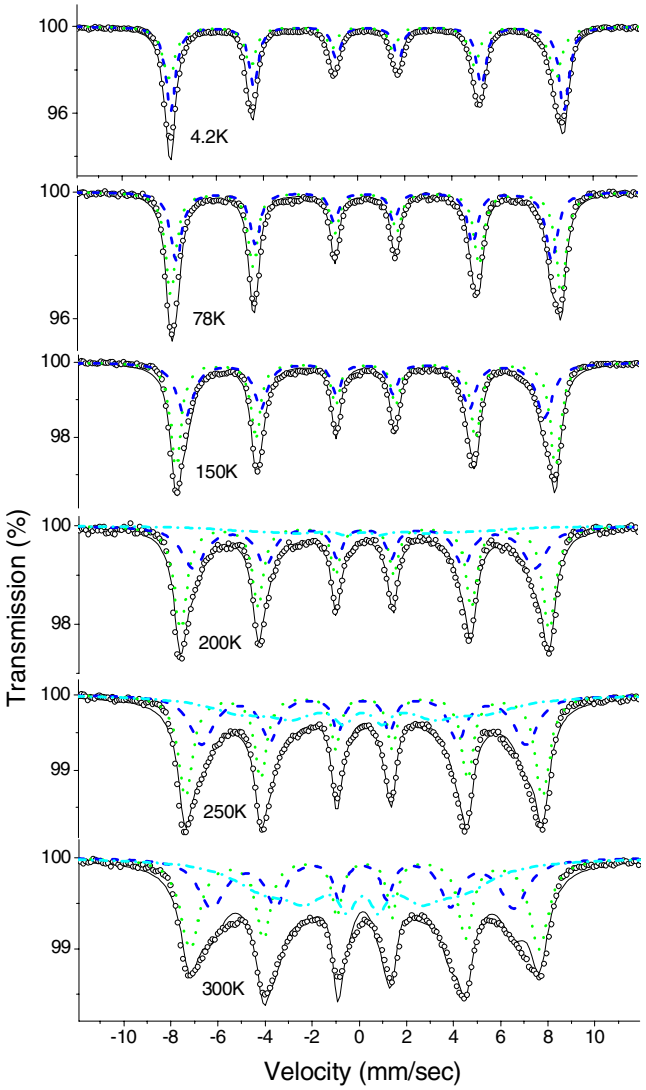

FIG. 7. (Color online) Mössbauer spectra of 12.5 nm γ-Fe_2O_3 nanoparticles at various temperatures. Spectral deconvolution: (---, blue) (A) site, (···, green) [B] site, and (-·-·-, cyan) intermediate relaxation component. The overall spectral temperature profile is consistent with strongly interacting particles.

$$U_{ij} = (\mu_0/4\pi)[\vec{\mu}_i \cdot \vec{\mu}_j/r_{ij}^3 - 3(\vec{\mu}_i \cdot \vec{r}_{ij})(\vec{\mu}_j \cdot \vec{r}_{ij})/r_{ij}^5], \tag{4}$$

where r_{ij} is the interparticle separation distance, center to center. At high magnetic dilution, the large distance separating the particles renders this interaction negligible. In more magnetically concentrated samples, the presence of this interaction will alter the superparamagnetic anisotropy energy barrier and cause a shift in the blocking temperature of the ZFC curve. The direction of the shift has been a matter of controversy.[38,39] Most experimental studies have observed a shift of the superparamagnetic blocking temperature to higher temperatures with increasing magnetic-particle concentration, in agreement with a dynamic study of interacting particles by Dormann *et al.*[38] However, there has also been one Mössbauer study by Mørup and Tronc,[39] whereby at least in the regime of weak dipolar interparticle interactions, a shift to lower temperatures has been observed and theoreti-

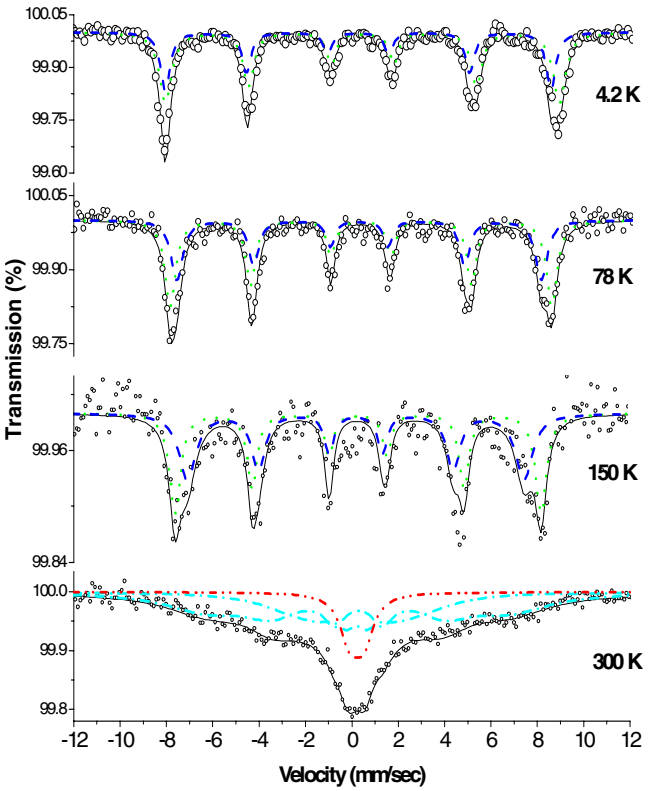

FIG. 8. (Color online) Mössbauer spectra of 12.5 nm γ-Fe_2O_3 nanoparticles coated with a 25-nm-thick SiO_2 shell at various temperatures. Spectral deconvolution: (---, blue) (A) site, (···, green) [B] site, and (-·--/-···--, cyan/red) intermediate/fast relaxation components.

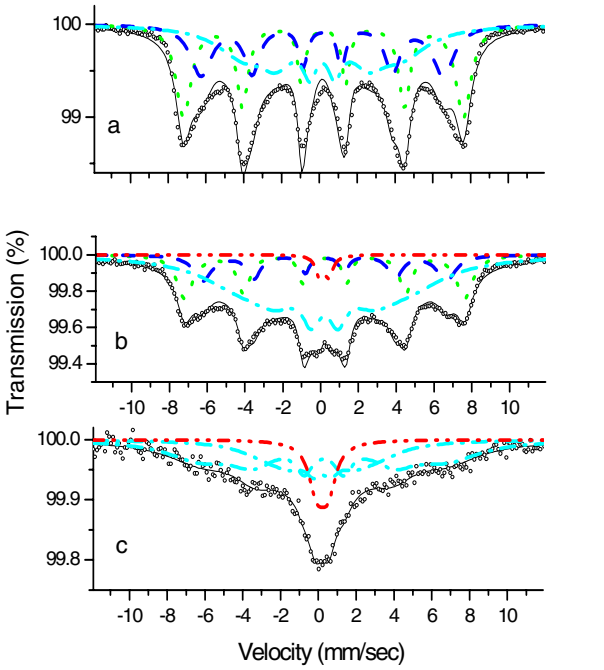

FIG. 9. (Color online) Room-temperature Mössbauer spectra of 12.5 nm γ-Fe_2O_3 nanoparticles with (a) no SiO_2 shell, (b) 4-nm-thick SiO_2 shell, and (c) 25-nm-thick SiO_2 shell. Spectral deconvolution: (---, blue) (A) site, (···, green) [B] site, and (-·--/-···--, cyan/red) intermediate/fast relaxation components.

cally supported.[40] This has prompted further studies resulting in a number of advanced theoretical models to better understand the dipole-dipole interaction in random anisotropy and textured samples in the presence and absence of external magnetic fields and particle-size distributions.[41–44] We note that precise analytical modeling of the interaction is, however, hindered by the complexity of the problem. For this reason, some investigators have combined analytical computations of the magnetization of interacting particles with numerical Monte Carlo simulations.[45]

In our experimental data, a monotonic shift of the ZFC maximum to higher temperatures was observed with increasing magnetic concentration, indicating an increase in the superparamagnetic anisotropy barrier. Monte Carlo calculations, currently being conducted on these systems in collaboration with Trohidou *et al.*,[46] concur with this result. We thus discuss our magnetization data assuming a simplified model, in which the anisotropy barrier is increased according to

$$T_{\max} = T_B = [(K_{\text{eff}}V_m + U_{\text{int}})/k_B]/\ln(\tau_m/\tau_0), \qquad (5)$$

where U_{int} is positive and gives a measure of the average effective interparticle interaction energy within the particle assembly. This equation is valid only for weakly interacting particles, i.e., for small values of the interaction energy as compared to the uniaxial magnetic anisotropy energy of the particle ($U_{\text{int}} < K_{\text{eff}}V_m$). Under this condition, $T_{\max}$ would fall close to T_B, which is the case for isolated magnetic particles. However, for large particle moments and small separations between particles, U_{int} can lead to collective magnetic phenomena and spin-glass-like magnetic ordering at a temperature $T_{\max} = U_{\text{int}}/k_B$. Thus, in the case of strongly interacting particles, $T_{\max}$ would give a measure of the magnetic ordering temperature of the system of particles,[25–28] rather than the superparamagnetic blocking temperature of the individual particle's magnetic moments.

The magnetic behavior of the samples studied here fell into four groups: (i) strongly interacting, (ii) intermediate interacting, (iii) weakly interacting, and (iv) isolated magnetic particles. $T_{\max}$ diminished gradually with increasing magnetic isolation, or decreasing magnetic volume fraction, from above room temperature for the bare particles to 75 K for the particles with the thickest coating (Table I). Magnetic interactions between the bare particles were strong, originating from the strong dipole-dipole interactions due to the proximity of adjacent particle's magnetic centers. The existence of exchange interactions across grain boundaries was minimized due to the fact that the bare particles in our samples referred to magnetic particles without any SiO_2 coating but capped, nevertheless, with a thin layer of oleic acid. The oleic acid was sufficient to prevent magnetic exchange interactions across the particle boundaries [see Fig. 2(b)], except possibly at points of incomplete or partial capping. Thus, we proposed that the magnetic behavior of these samples reflected primarily the single-particle anisotropy and the effect of strong dipolar interactions.

The presence of strong interparticle magnetic interactions in the bare particles (sample A) was inferred by the following

experimental evidence in the magnetization data [Fig. 11]: (i) the branching (or bifurcation) of the ZFC and FC data occurred at a high temperature, (ii) the branching off temperature, T_{Br}, coincided with the temperature of maximum magnetization in the ZFC curve, and (iii) the FC curve already showed magnetic saturation upon bifurcation.[47]

Sample B contained particles with a 12.5 nm magnetic core coated with a 4-nm-thick silica shell. Dipole-dipole interactions were somewhat diminished relative to sample A, while exchange interactions were obviated by the silica shell. The reduced strength of interparticle dipolar interactions resulted in a reduced value of T_{max} (175 K), and its clear separation from $T_{Br}=185$ K, but the interparticle interactions still remained fairly strong [Fig. 11]. T_{max} in the data for samples A and B shown in Fig. 11 must, therefore, be associated with an ordering temperature, rather than a SP blocking temperature; i.e., these systems of strongly interacting magnetic particles of random anisotropy displayed a spin-glass-like magnetic phase transition.[25–28]

The addition of increasingly thicker coatings of 25, 35, and 46 nm for samples C, D, and E, respectively, further increased the degree of magnetic isolation of the γ-Fe_2O_3 cores, corresponding to magnetic volume fractions of 0.008, 0.003, and 0.002, respectively. As the separation between magnetic centers increased, T_{max} continued to decrease, while the difference between T_{max} and T_{Br} increased [Fig. 11, Table I]. The FC magnetization continued to increase for a while with decreasing temperature below T_{Br}, before it leveled off to saturation at lower temperatures. The magnetic behavior became increasingly characteristic of weakly interacting or isolated magnetic particles, where $T_{max} \rightarrow T_B$. The maximum in the ZFC magnetization leveled off at $T_{max}=75$ K (Fig. 11, Table I). Assuming that for the most magnetically dilute sample (sample E) with an interparticle distance $r=104.5$ nm (Table I), magnetic centers were isolated; the blocking temperature was estimated at $T_B=75$ K. Below this temperature, the magnetization vectors of individual particles were blocked from thermally driven Néel-type relaxation spin reversals[13] along opposite directions of the easy axis of magnetization. The data of sample E, for which $T_{max}=T_B$, gave a measure of the effective magnetic anisotropy energy density of individual particles. Using Eq. (3) and assuming $\tau_0=10^{-9}$ s and a magnetization characteristic measuring time $\tau_{mag}=10$ s, the magnetic anisotropy energy density was estimated at $K_{eff}=2.37\times10^4$ J/m^3, which was five times larger than the magnetocrystalline anisotropy constant of bulk maghemite, $K_{mc}=0.47\times10^4$ J/m^3.[48] This increase was attributed to surface and strain effects that dominate the magnetic anisotropy density in small particles. This value also followed the trend recently shown by Rebbouh *et al.*[27] for maghemite nanoparticles with diameters of 4, 7, 9, and 11 nm.

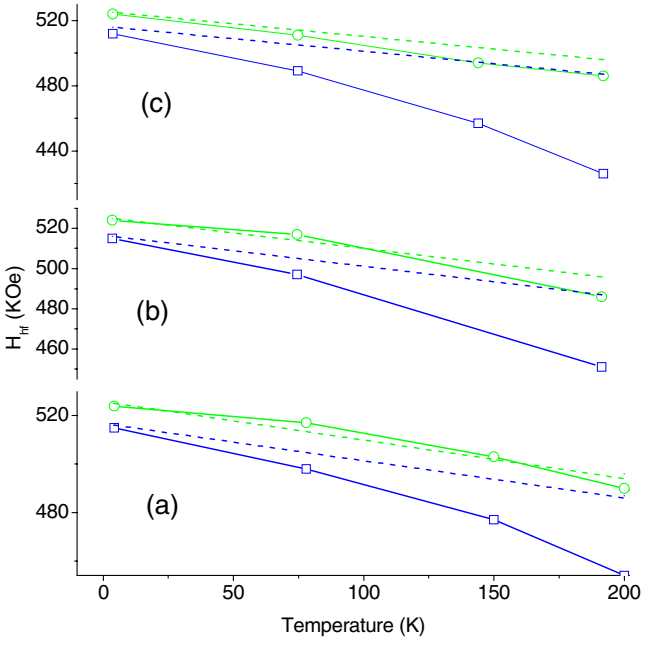

FIG. 10. (Color online) Temperature variation of the hyperfine field (H_{hf}) for the (—, blue squares) (A) site and (—, green circles) [B] site of the 12.5-nm γ-Fe_2O_3 nanoparticles with (a) no SiO_2 shell (sample A), (b) 4-nm-thick SiO_2 shell (sample B), and (c) 25-nm-thick SiO_2 shell (sample C). The initial slope (dashed lines) was predicted by the CME model for the (---, blue) (A) sites and (---, green) [B] sites of noninteracting particles (see Table II).

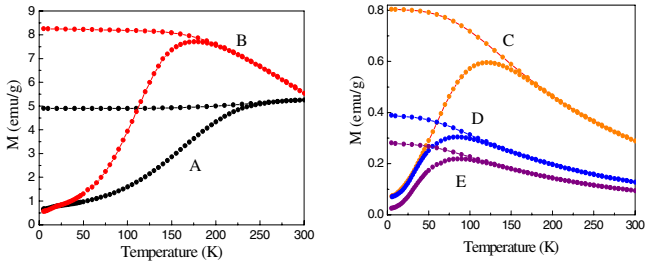

FIG. 11. (Color online) ZFC and FC magnetization measurements of 12.5 nm γ-Fe_2O_3 nanoparticles with (A) no SiO_2 shell, (B) 4-nm-thick solid SiO_2 shell and 25-nm-thick solid SiO_2 shell, (C) without, and with (D) 10-nm-thick and (E) 21-nm-thick mesoporous silica shells. Applied field=50 Oe.

We note that due to the different characteristic times of Mössbauer and magnetization measurements ($\tau_{möss}=10^{-8}$ s and $\tau_{mag}=10$ s, respectively), the Mössbauer blocking temperature for the same sample of particles was expected to be higher than that for magnetization measurements, i.e., $T_{Bmag}/T_{Bmöss}=0.35$.[49] This would predict a Mössbauer blocking temperature of 215 K for the isolated 12.5 nm γ-Fe_2O_3 nanoparticles with T_{Bmag} of 75 K, consistent with the Mössbauer data of Fig. 8, and would indicate that the onset of the collapse of the six-line magnetic spectrum for the particles with 25-nm-thick SiO_2 coating should occur between 150 K and room temperature.

Use of Eq. (5) to obtain an estimate of U_{int} in the noniso-lated particle assembly of sample D indicated a value of $U_{int}=2.6\times10^{-22}$ J, which was about 2 orders of magnitude smaller than the magnetic anisotropy energy of the particles $E_{ani}=K_{eff}V_m=2.42\times10^{-20}$ J. We could therefore assume that the interparticle interaction energy in sample D was weak. However, for sample C, the value of the dipole-dipole interaction estimated in this way (1.4×10^{-20} J) was of the same order of magnitude as the anisotropy energy of the particle. Thus, for samples A–C, the interaction energy could not be

considered a small perturbation to the anisotropy energy, and thus, the simplified theory for interparticle interactions reflected in Eq. (5), which assumed weakly interacting particles, was not applicable here. With increasing magnetic volume fraction, U_{int} became increasingly dominant, leading to spin-glass-like magnetic ordering at $T_{\max}$. This ordering temperature was technique independent and, thus, both magnetization and Mössbauer measurements indicated an ordering temperature above room temperature for the bare particle assembly of sample A ($T_{\max} > 300$ K).

Returning to the temperature-dependent Mössbauer spectra of Figs. 7 and 8, it was observed that the decrease in the internal hyperfine fields at the iron sites with increasing temperature was steeper for the more magnetically isolated particles. This is clear from the data in Table II and Fig. 10, where the hyperfine fields at the tetrahedral (A) and octahedral [B] iron sites are plotted against temperature. Our data deviated from the linear decrease in magnetic field [Eq. (1)] predicted by the CME model of Mørup and Topsøe[35] for isolated superparamagnetic particles, presumably, due to the presence of interparticle interactions. To a first approximation, the CME model has been extended to predict the temperature dependence of the hyperfine field in the presence of interparticle interactions by adding an energy term U_{int} to the particle's magnetic anisotropy energy, according to Eq. (6) below,[24]

$$H_{\text{hf}}(T) = H_{\text{hf}}^{0}[1 - k_B T/(2K_{\text{eff}}V_m + U_{\text{int}})]. \tag{6}$$

As U_{int} may be temperature dependent, due to thermal fluctuations of the direction of the particle's magnetic moment, Eq. (6) would not necessarily predict a linear decrease in hyperfine field, as we observed experimentally. Ignoring its temperature dependence over a short temperature range, the initial slope at 4.2 K is obtained as follows:

$$\Delta H_{\text{hf}}/\Delta T = -H_{\text{hf}}^{0}k_B/(2K_{\text{eff}}V_m + U_{\text{int}}), \tag{7}$$

where U_{int} is assumed constant. Thus, for an interacting system of particles with positive U_{int}, the initial slope in hyperfine field reduction should be less steep than that predicted by the CME model.

The experimental initial slopes, $\Delta H_{\text{hf}}/\Delta T$ at 4.2 K, of our samples were compared with that expected for isolated particles according to the CME model. Figure 10 shows the linear reduction with increasing temperature in (A) and [B] site hyperfine fields for the isolated particles predicted by the CME model, together with the experimental data for samples A–C taken from Table II. It was clear that the initial slope of the [B] subsites of samples A and B (−0.095 kOe/K) showed a less steep reduction in magnetic hyperfine field value with increasing temperature compared to the CME model's slope (−0.150 kOe/K), as expected from Eq. (7) for positive values of U_{int}, while for sample C, the slope equaled that of the CME model's prediction. Surprisingly, the (A) subsites displayed a considerably faster decrease in the hyperfine field values with increasing temperature for all three samples compared to the CME model's predictions.

We attributed this discrepancy to a contribution from surface iron sites. The CME model assumes uniaxial anisotropy, leading to a double potential well with global-energy minima for the particle's total magnetic moment, or macrospin, oriented along or opposite the anisotropy axis.[35] Collective magnetic excitations account for the precession or oscillations of the particle's macrospin about its magnetic easy axis, triggered at low temperatures by thermal energies insufficient to induce spin flips between opposite directions of the anisotropy axis, for $k_B T < K_{\text{eff}}V_m$. However, the particle surface-energy landscape can accommodate additional local minima due to lower iron coordination, surface strain and spin canting associated with the surface. Many studies indicate that the breakage of superexchange bonds results in the creation of a surface shell within which spin disorder leads to a spin-glass-like phase at the surface with closely spaced equilibrium states.[50,51] This surface shell may penetrate quite far into the interior of the particle and may be uncoupled from the core, behaving as a quasi-independent layer.[52–54] This introduces greater complexity in the potential-energy landscape at the surface, which in turn supports low-energy spin-wave excitations. This is consistent with recent theoretical calculations that take into account surface anisotropy in spherical many-spin magnetic particles,[55,56] which indicate that the surface introduces a cubic anisotropy component to the energy landscape. Such surface spin excitations leading to a sharp decline of hyperfine fields at the surface have previously been observed in antiferromagnetic nanoparticles.[57] Faster spin fluctuations at the surface compared to the core have also recently been reported for 7-nm-diam γ-Fe_2O_3 nanoparticles by Desautels *et al.*[58,59]

Accordingly, surface sites in our composite nanoparticles would be expected to show a rapid decay in hyperfine field values with increasing temperature. In the Mössbauer spectral fitting, these surface sites, due to their lower symmetry, behaved more like the (A) sites due to their lower degree of coordination. The data indicated the onset of relaxation of the surface shell even at 78 K. Such sites could produce the broad intermediate relaxation components in the fitting of spectra shown in Figs. 7–9 at temperatures above 200 K (see above). This surface relaxation mechanism would further enhance the line broadening generally arising from spin-glass dynamics in these strongly interacting nanoparticle systems, with the wide distribution of relaxation times associated with spin glasses[60] giving rise to the broad intermediate relaxation component observed in the Mössbauer spectra with increasing temperature.

IV. CONCLUSION

Magnetization and Mössbauer data on single-crystalline monodispersed γ-Fe_2O_3 nanoparticles coated with SiO_2 and mesoporous silica with well-controlled nearest-neighbor interparticle distances are presented. A gradual transition from a strongly dipolar interacting spin-glass-type system to isolated superparamagnetic particle system is observed, with the $T_{\max}$ from ZFC magnetization measurements increasing with increased interparticle interaction strength. At low temperatures (~4.2 K), the initial slope in the temperature dependence of the hyperfine magnetic field of the octahedral [B]

sites of the maghemite spinel structure in magnetically dense samples agrees qualitatively with the CME model, as extended to weakly interacting particles with positive average interparticle interaction energy. In contrast, the tetrahedral (A) sites' subspectra show the opposite effect, indicating that the distorted surface iron sites in the magnetic nanoparticles' outer layers behave more like (A) iron sites than [B] iron sites.

ACKNOWLEDGMENTS

This work was funded by the European Union Marie Curie Program at NCSR "Demokritos," the National Science Foundation under Grant No. DMR 0604049 at Villanova University, and the Institute of Bioengineering and Nanotechnology (Biomedical Research Council, Agency for Science, Technology and Research, Singapore).

*Corresponding author; gcp@villanova.edu
†Deceased.
‡Present address: College of Bionanotechnology, Gachon Bionano Research Institute, Kyungwon University, Sungnam, Korea.

[1] *Nanoparticles: From Theory to Application*, edited by G. Schmid (Wiley, Weinheim, 2004).
[2] H. Gleiter, Nanostruct. Mater. **1**, 1 (1992).
[3] A.-H. Lu, E. L. Salabas, and F. Schüth, Angew. Chem., Int. Ed. **46**, 1222 (2007).
[4] L. E. Euliss, J. A. DuPont, S. Gratton, and J. DeSimone, Chem. Soc. Rev. **35**, 1095 (2006).
[5] C. Ross, Annu. Rev. Mater. Res. **31**, 203 (2001).
[6] U. Häfeli, W. Schutt, J. Teller, and M. Zborowski, *Scientific and Clinical Applications of Magnetic Carriers* (Plenum, New York, 1998).
[7] F. C. Meldrum, B. R. Heywood, and S. Mann, Science **257**, 522 (1992).
[8] L. E. Euliss, S. G. Grancharov, S. O'Brien, T. J. Deming, G. D. Stucky, C. B. Murray, and G. A. Held, Nano Lett. **3**, 1489 (2003).
[9] J. M. Coey, Phys. Rev. Lett. **27**, 1140 (1971).
[10] F. T. Parker and A. E. Berkowitz, Phys. Rev. B **44**, 7437 (1991).
[11] A. Millan, A. Urtizberea, N. J. O. Silva, F. Palacio, V. S. Amaral, E. Snoeck, and V. Serin, J. Magn. Magn. Mater. **312**, L5 (2007).
[12] O. Helgason, H. K. Rasmussen, and S. Mørup, J. Magn. Magn. Mater. **302**, 413 (2006).
[13] L. Néel, Ann. Geophys. (C.N.R.S.) **5**, 99 (1949).
[14] W. F. Brown, Jr., Phys. Rev. **130**, 1677 (1963); J. Appl. Phys. **39**, 993 (1968).
[15] A. Aharoni, in *Magnetic Properties of Fine Particles*, edited by J. L. Dormann and D. Fiorani (Elsevier Science, North-Holland, 1991), p. 3.
[16] E. C. Stoner and E. P. Wohlfarth, Philos. Trans. R. Soc. London, Ser. A **240**, 599 (1948); IEEE Trans, Magn. **27**, 3475 (1991).
[17] S. Gider, D. D. Awschalom, T. Douglas, S. Mann, and M. Chaparala, Science **268**, 77 (1995).
[18] E. M. Chudnovsky and L. Gunther, Phys. Rev. Lett. **60**, 661 (1988).
[19] W. Wernsdorfer, E. B. Orozco, K. Hasselbach, A. Benoit, B. Barbara, N. Demoncy, A. Loiseau, H. Pascard, and D. Mailly, Phys. Rev. Lett. **78**, 1791 (1997).
[20] W. Wernsdorfer, E. Bonet Orozco, K. Hasselbach, A. Benoit, D. Mailly, O. Kubo, H. Nakano, and B. Barbara, Phys. Rev. Lett. **79**, 4014 (1997).
[21] R. Skomski, J. Phys.: Condens. Matter **15**, R841 (2003).
[22] J. Park, J. Joo, S. G. Kwon, Y. Jang, and T. Hyeon, Angew. Chem., Int. Ed. **46**, 4630 (2007).
[23] S. Mørup, C. A. Oxborrow, P. V. Hendriksen, M. S. Pedersen, M. Hanson, and C. Johansson, J. Magn. Magn. Mater. **140-144**, 409 (1995).
[24] S. Mørup, D. E. Madsen, C. Frandsen, C. R. H. Bahl, and M. F. Hansen, J. Phys.: Condens. Matter **19**, 213202 (2007).
[25] S. Mørup, F. Bødker, P. V. Hendriksen, and S. Linderoth, Phys. Rev. B **52**, 287 (1995).
[26] S. Mørup, Europhys. Lett. **28**, 671 (1994).
[27] L. Rebbouh, R. P. Hermann, F. Grandjean, T. Hyeon, K. An, A. Amato, and G. J. Long, Phys. Rev. B **76**, 174422 (2007).
[28] W. Luo, S. R. Nagel, T. F. Rosenbaum, and R. E. Rosensweig, Phys. Rev. Lett. **67**, 2721 (1991).
[29] C. Binns, M. J. Maher, Q. A. Pankhurst, D. Kechrakos, and K. N. Trohidou, Phys. Rev. B **66**, 184413 (2002).
[30] J. A. De Toro, J. P. Andrés, J. A. González, J. P. Goff, A. J. Barbero, and J. M. Riveiro, Phys. Rev. B **70**, 224412 (2004).
[31] J. Du, B. Zhang, R. K. Zheng, and X. X. Zhang, Phys. Rev. B **75**, 014415 (2007).
[32] D. K. Yi, S. S. Lee, G. C. Papaefthymiou, and J. Y. Ying, Chem. Mater. **18**, 614 (2006).
[33] T. Hyeon, S. S. Lee, J. Park, Y. Chung, and H. B. Na, J. Am. Chem. Soc. **123**, 12798 (2001).
[34] N. N. Greenwood and T. C. Gibb, *Mössbauer Spectroscopy* (Chapman and Hall, London, 1971).
[35] S. Mørup and H. Topsøe, Appl. Phys. (Berlin) **11**, 63 (1976).
[36] D. P. E. Dickson, N. M. K. Reid, C. Hunt, H. D. Williams, M. El-Hilo, and K. O'Grady, J. Magn. Magn. Mater. **125**, 345 (1993).
[37] A. H. Morrish, *The Principles of Magnetism* (reprinted by Institute of Electrical and Electronics Engineers, New York, 2001), p. 476.
[38] J. L. Dormann, L. Bessais, and D. Fiorani, J. Phys. C **21**, 2015 (1988).
[39] S. Mørup and E. Tronc, Phys. Rev. Lett. **72**, 3278 (1994).
[40] M. F. Hansen and S. Mørup, J. Magn. Magn. Mater. **184**, L262 (1998).
[41] P. E. Jönsson and J. L. Garcia-Palacios, Europhys. Lett. **55**, 418 (2001).
[42] J. L. Garcia-Palacios and D. A. Garanin, Phys. Rev. B **70**, 064415 (2004).
[43] M. Azeggagh and H. Kachkachi, Phys. Rev. B **75**, 174410 (2007).
[44] R. Sappey, E. Vincent, N. Hadacek, F. Chaput, J. P. Boilot, and D. Zins, Phys. Rev. B **56**, 14551 (1997).
[45] H. Kachkachi and M. Azeggagh, Eur. Phys. J. B **44**, 299 (2005).
[46] K. N. Trohidou, M. Vasilakaki, E. Devlin, G. C. Papaefthymiou, D. K. Yi, S. N. Riduan, S. S. Lee, and J. Y. Ying (unpublished).
[47] P. Prene, E. Tronc, J.-P. Jolivet, J. Livage, R. Cherkaoui, M. Nogues, J. L. Dorman, and D. Fiorani, IEEE Trans. Magn. **29**,

2658 (1993).
[48] S. Kripicka and K. Zaveta, in *Magnetic Oxides Part I*, edited by D. J. Craik (Wiley-Interscience, New York, 1975).
[49] G. Xiao, S. H. Liou, A. Levy, J. N. Taylor, and C. L. Chien, Phys. Rev. B **34**, 7573 (1986).
[50] P. V. Hendriksen, S. Linderoth, and P.-A. Lindgård, Phys. Rev. B **48**, 7259 (1993).
[51] R. H. Kodama, A. E. Berkowitz, E. J. McNiff, Jr., and S. Foner, Phys. Rev. Lett. **77**, 394 (1996).
[52] B. Martinez, X. Obradors, L. Balcells, A. Rouanet, and C. Monty, Phys. Rev. Lett. **80**, 181 (1998).
[53] G. H. Kachkachi and D. A. Garanin, Physica A **300**, 487 (2001).
[54] O. Iglesias, F. Ritort, and A. Labarta, arXiv:cond-mat/0008312, presented at NATO-ASI Workshop in Rodos (Greece): Magnetic Storage Systems beyond 2000. NATO-ASI Series, Kluwer editors (Series II, Vol. 41) (2000).
[55] H. Kachkachi and E. Bonet, Phys. Rev. B **73**, 224402 (2006).
[56] H. Kachkachi and D. A. Garanin, in *Surface Effects in Magnetic Nanoparticles*, Book Series in Nanostructure Science and Technology, edited by D. Fiorani (Springer, New York, 2005), p. 75; H. Kachkachi and D. A. Garanin, arXiv:cond-mat/0310694 (unpublished).
[57] F. Bou-Abdallah, E. Carney, N. D. Chasteen, P. Arosio, A. J. Viescas, and G. C. Papaefthymiou, Biophys. Chem. **130**, 114 (2007).
[58] R. D. Desautels, E. Skoropala and J. van Lierop, J. Appl. Phys. **103**, 07D512 (2008).
[59] T. N. Shendruk, R. D. Desautels, B. W. Southern, and J. van Lierop, Nanotechnology **18**, 455704 (2007).
[60] A. P. Murani, J. Magn. Magn. Mater. **22**, 271 (1981).